The Realization of an Earthquake Early Warning System for Schools and Its Performance during the 2019 M_L 6.3 Hualien (Taiwan) Earthquake

Ting-Yu Hsu[*1,2,3], Chun-Hsiang Kuo[4], Hsiu-Hsien Wang[2], Yu-Wen Chang[2], Pei-Yang Lin[2], and Kuo-Liang Wen[4]

Abstract

This article discusses the earthquake early warning system (EEWS) for schools of the National Center for Research on Earthquake Engineering, Taiwan (NCREE's EEWS, earthquake early warning system [NEEWS]) that was recently completed. The system consists of 98 seismic stations with a complete set of system capabilities and 3514 broadcast stations with only the associated alert broadcast system capabilities. The broadcast stations receive both any on-site alerts issued by the seismic stations and any regional alerts issued by the Central Weather Bureau and then broadcast whatever alert is received earliest. Shortly after the establishment of the NEEWS, the M_L 6.3 Hualien earthquake, which had a maximum measured peak ground acceleration (PGA) of 515.17 Gal, struck Taiwan on 18 April 2019. During the earthquake, the performance of both the seismic stations and the broadcast stations of the system was documented. The current study analyzes and discusses the accuracy of the PGA predictions, lead times, and classification performance at both the seismic stations and the broadcast stations of the NEEWS. The results show that the NEEWS is a cost-effective and promising system of EEW.

Cite this article as Hsu, T.-Y., C.-H. Kuo, H.-H. Wang, Y.-W. Chang, P.-Y. Lin, and K.-L. Wen (2020). The Realization of an Earthquake Early Warning System for Schools and Its Performance during the 2019 M_L 6.3 Hualien (Taiwan) Earthquake, *Seismol. Res. Lett.* **92**, 342–351, doi: 10.1785/0220190329.

Introduction

Because Taiwan has experienced serious damage from several destructive in-land and offshore earthquakes, earthquake early warning (EEW) becomes one of the solutions to reduce seismic loss. In addition, many school buildings were damaged during the 1999 Chi-Chi, Taiwan, earthquake. Therefore, the National Center for Research on Earthquake Engineering (NCREE), Taiwan, began establishing an EEW system (EEWS) for schools in 2009 by first utilizing a limited budget to establish several stations at elementary schools. The NCREE's EEWS is called the earthquake early warning system (NEEWS). Based on the fact that during several moderate earthquakes that occurred in 2013, the NEEWS successfully provided timely warnings before the strong waves struck the schools, the Taiwan government asked the NCREE to expand the NEEWS to all of the public elementary and junior high schools in Taiwan. Because the total number of these public schools was quite large, approximately 3500, a cost-effective solution was required. As a result, a satellite-based approach was implemented. Specifically, a total of 98 seismic stations and 3514 broadcast stations were constructed at the schools. The seismic stations were furnished with the complete set of NEEWS equipment, including seismographs, a data logger, a computer, an alert broadcast system, and an uninterruptible power supply, whereas the broadcast stations were equipped with only the alert broadcast system. Each broadcast station receives any alerts issued by the three predesignated seismic stations at the shortest distances from it using the on-site approach (Hsu *et al.*, 2013) and the regional alerts issued by the Central Weather Bureau (CWB) (Chen, Hsiao, and Wu, 2015), and then broadcasts whichever alert is received earliest. The locations of the seismic stations were selected so that they would be roughly uniformly distributed throughout the areas with schools.

To ensure that alert information is distributed to the broadcast stations throughout the network with little delay, a private network maintained by a private company, Chunghwa Telecom, was implemented. To reduce the number of triggers of the NEEWS caused by non-earthquake events, two seismographs are installed at different locations for each seismic

1. Department of Civil and Construction Engineering, National Taiwan University of Science and Technology, Taipei City, Taiwan; 2. National Center for Research on Earthquake Engineering, Taipei City, Taiwan; 3. Taiwan Building Technology Center, National Taiwan University of Science and Technology, Taipei City, Taiwan; 4. Department of Earth Science, National Central University, Taoyuan City, Taiwan

*Corresponding author: tyhsu@ntust.edu.tw

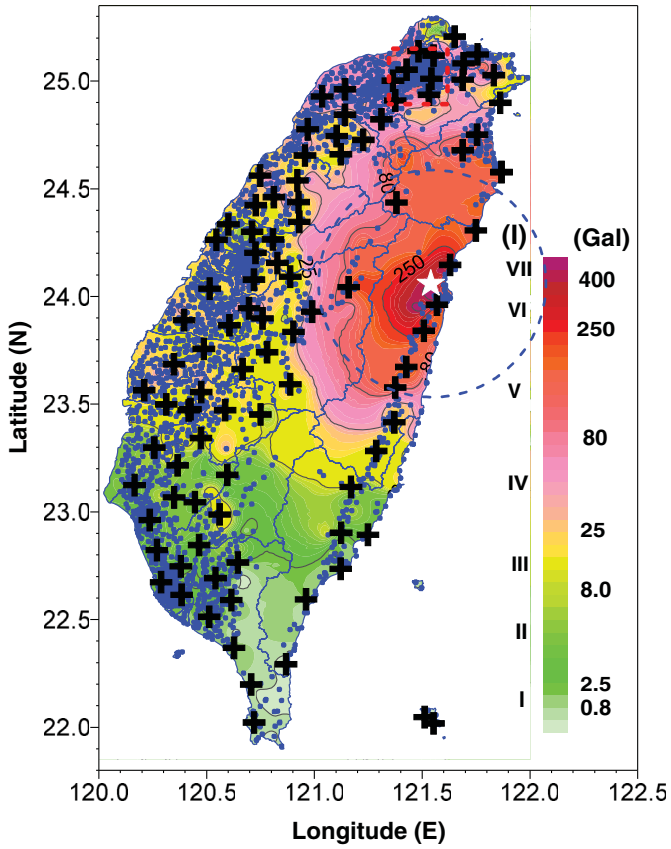

Figure 1. Locations of the 98 National Center for Research on Earthquake Engineering's NCREE's earthquake early warning system (NEEWS) seismic stations (black crosses) and 3514 broadcast stations (blue dots), as well as the location of the epicenter of the 2019 Hualien earthquake (star) and the Central Weather Bureau (CWB) intensity scale (scale bar). Circle with a radius of 54 km roughly depicts the observed region in which the on-site approach was faster than the CWB regional approach. The location of Taipei is indicated by the red rectangular box.

station. Only when both seismographs trigger does the seismic station recognize a given event as an earthquake event.

A number of on-site EEW approaches have been developed recently (Nakamura, 1998; Odaka *et al.*, 2003; Kanamori, 2005; Allen *et al.*, 2009; Zollo *et al.*, 2010; Böse *et al.*, 2012; Carranza *et al.*, 2013; Hsu *et al.*, 2013; Wu *et al.*, 2013; Peng *et al.*, 2015; Emolo *et al.*, 2016; Caruso *et al.*, 2017), and some of them have been implemented in EEWSs around the world. More information about the recent status of these EEWSs can be found in Allen and Melgar (2019). The on-site NEEWS for Taiwan estimates the peak ground acceleration (PGA) of a coming earthquake by relying on support vector machine techniques recently developed by Hsu *et al.* (2013). The PGA is predicted based on six *P*-wave features including the peak acceleration, peak velocity, peak displacement, effective predominant period, cumulative absolute velocity, and the integral of the squared velocity extracted from the first 3 s of the measured vertical acceleration of a single station.

During the construction of the NEEWS, the NEEWS experienced the M_w 6.5 Meinong earthquake in 2016 and the M_w 6.4 Hualien earthquake in 2018. The NEEWS performed well during both of these events (Hsu *et al.*, 2016, 2018). The on-site NEEWS successfully provided 3.2–12.8 s of lead time (LT) for the stations with PGA ≥ 80 Gal during these two earthquakes. The construction of the NEEWS was finished in early April of 2019. Soon afterward, on 18 April 2019, another Hualien earthquake ($M_L = 6.3$, $M_w = 6.2$) occurred at 13:01 p.m. local time (5:01 p.m. UTC) at 24.06° N Latitude and 121.54° E Longitude, with a focal depth of 20.3 km, and resulted in one death and nonstructural damage to several buildings (the locations of stations of the NEEWS and the epicenter of the 2019 Hualien earthquake are marked in Fig. 1). This moderate earthquake provided a precious opportunity for an inspection of the in situ performance of the NEEWS. Therefore, this study aims to illustrate how the NEEWS functions, especially at the broadcast stations, using the 2019 Hualien earthquake as the case study.

Nonstructural damage to several buildings in Taipei, which is the economic center of Taiwan with a population of 6.6 million, was reported during this event (the location of Taipei city is marked in Fig. 1). Historically, on 20 May 1986, an earthquake of $M_L = 6.5$ occurred near the epicenter of the 2019 event and caused serious damage to two school buildings in Taipei, whereas the two offshore Hualien earthquakes (both $M_L = 6.8$) that occurred on 15 November 1986, and 31 March 2002, and the 1999 Chi-Chi earthquake ($M_w = 7.6$) also caused severe damage in Taipei. These events, which all had epicentral distances of more than 70 km from Taipei, induced building damage due to basin effects. In this study, therefore, we also want to investigate whether the NEEWS was able to issue alerts efficiently for the vulnerable capital of Taipei during the remote 2019 Hualien earthquake.

2019 Hualien Earthquake Data

During the 2019 Hualien earthquake, 37, 106, 631, and 68 valid accelerograms were recorded by the Seismic Array of NCREE (SANTA) stations (Kuo *et al.*, 2019), the CWB real-time data stream (RTD) stations (Wu *et al.*, 2000), the P-Alert Strong Motion Network (Chen, Wu, and Chin, 2015), and the NEEWS stations of NCREE (Hsu *et al.*, 2018), respectively (see Data and Resources section). The largest measured horizontal PGA value was 515.17 Gal at the CWB East Tong Men station, which had a 12 km epicentral distance. Based on the focal mechanism solutions issued by the CWB, the two nodal planes of the earthquake were 64°/25°/122° and 209°/69°/76°. Figure 1 shows the observed PGA distribution of the aforementioned stations. The locations of the seismic stations and broadcast stations of the NEEWS are also marked with black crosses and blue dots, respectively, in the same figure.

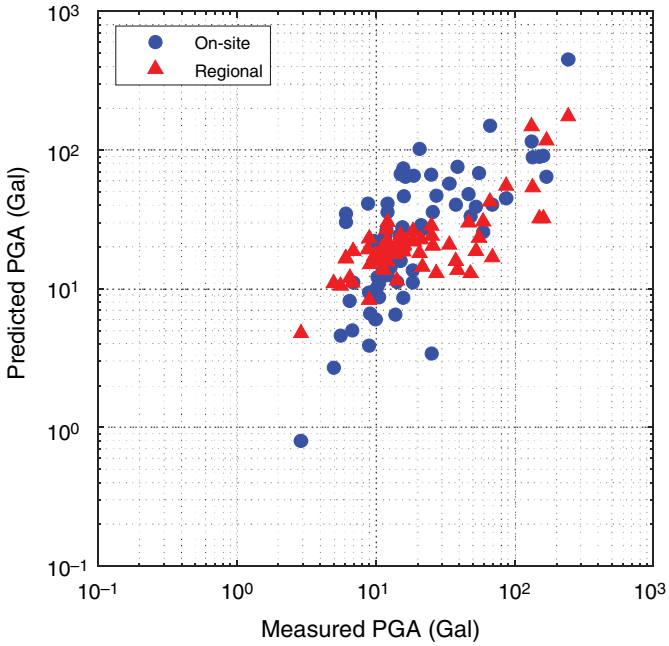

Figure 2. Comparison of the predicted peak ground acceleration (PGA) and observed PGA values for the 68 NEEWS seismic stations.

It took 14 s for the CWB regional EEWS to issue an alert after the 2019 Hualien earthquake occurred.

PGA Prediction and LT

The predicted PGA values of the 68 NEEWS seismic stations during the 2019 Hualien earthquake are shown in Figure 2. Both the PGA values predicted by the on-site approach and the regional CWB approach are illustrated on a logarithmic scale. The standard deviations of the logarithm PGA residuals using the on-site approach and the regional approach were approximately 0.57 and 0.64, respectively. In general, the accuracy of both the on-site and regional approaches is quite high. Basic information, as well as the performance metrics for these stations, are listed in Table 1. To have a rough idea of how good the performance of PGA prediction is, the standard deviation of the logarithm PGA residuals when establishing the general attenuation law of horizontal PGA at hard rock sites in Taiwan is employed (Jean *et al.*, 2006). The standard deviation of the logarithm PGA residuals of the attenuation law is 0.78, and the ones of both the on-site approach and the regional approach during the 2019 Hualien earthquake were even lower.

In Taiwan, the CWB expresses seismic intensity in terms of an eight-level scale based on the measured PGA (Wu *et al.*, 2003) as illustrated in Figure 1. In this article, this CWB intensity scale is used. We define the intensity prediction accuracy ratio (IPAR) as the ratio of the predicted intensity scale located within a one-scale difference from the real intensity scale among all the considered earthquake data. Only the earthquake data with a measured intensity scale ≥ 4 or a predicted intensity scale ≥ 4 were considered. As a result, the IPAR for the on-site approach was 31/36 = 86.1%, whereas that of the CWB regional approach was 24/24 = 100%. As for the measured intensity scale ≥ 4, the median and standard deviations of the logarithm PGA residuals were 0.02 and 0.22 for the on-site approach and −0.29 and 0.22 for the regional approach, respectively. This indicated that the utilized on-site approach was quite reliable for the strong motion region in this earthquake event.

Figures 3 and 4 illustrate the measured acceleration time history at the 10 stations closest to the epicenter. For conciseness, only the horizontal component with the maximum PGA is plotted in sequence by the epicentral distance. The time at the trigger, *S*-wave arrival, and alert issuance of the on-site and regional approaches are also marked in the same figures. The current version of the on-site approach used the first 3 s after the *P*-wave arrival to predict the PGA for all the seismic stations, except Stations S046 and S049. These two stations employed a new version of the on-site algorithm which updated the predicted PGA every second, starting from only one second. The details of the algorithm can be found in Hsu *et al.* (2013).

A good EEWS needs both timeliness and accuracy. For timeliness, we consider the LT. LT is defined as the time difference between when a PGA prediction is first issued and the arrival of the *S* wave. At Station S019, with only a 9.7 km epicentral distance, the LT of the on-site approach was −0.6 s. At Stations S046 and S049, with epicentral distances of approximately 12.9 and 23.7 km, respectively, the LT values of the on-site approach were 1.7 and 4.2 s, respectively. These two stations issued their alerts only 1 s after the *P* arrival; otherwise, the LT of Station S046 could have been shorter or even negative. Meanwhile, even for Station S019, the LT could have been positive if the new version of the on-site algorithm had been employed. For the stations with a seismic intensity of *V* (i.e., S105, S006, S005, and S050) and epicentral distances of approximately 40–66 km, LT values of approximately 3–6 s were recorded. Figure 5 illustrates the relationships between the LT and the epicentral distance values of the on-site and regional approaches. In general, the LT increases with the epicentral distance. This figure clearly shows the advantage of the on-site stations (NEEWS) over the network-based EEW stations at short distances. The blue circle with a radius of 54 km in Figure 1 roughly depicts the observed region in which the on-site approach was faster than the regional approach. Evidently, the on-site approach can yield more LT for the areas with higher seismic intensity levels.

Classification Performance

For operational purposes, the threshold to issue an alert of the NEEWS was set to scale IV. The locations of the 36 NEEWS seismic stations with predicted intensity scale of ≥IV, and 2180 corresponding broadcast stations are shown in Figure 6. If an alert was issued before the threshold was reached, we

TABLE 1
Performance Summary of the 68 Seismic Stations of the NEEWS during the 2019 Hualien Earthquake

				LT (s)		PGAx (Gal)		Ix		
No.	***R* (km)**	**PGAr (Gal)**	**Ir**	**On-Site**	**Regional**	**On-Site**	**Regional**	**On-Site**	**Regional**	**Classification**
S019	9.7	243.1	5	–0.6	–7.0	450.6	174.9	7	5	TN
S046	12.9	132.3	5	1.7	–6.7	115.2	148.7	5	5	TP
S049	23.7	169.5	5	4.2	–3.2	116.7	116.7	5	5	TP
S105	40.8	86.9	5	3.1	0.8	55.2	55.2	4	4	TP
S006	43.8	134.9	5	3.9	1.7	88.6	54.0	5	4	TP
S117	46.6	66.6	4	2.8	1.2	150.1	42.6	5	4	TP
S048	55.5	59.3	4	6.3	5.5	30.4	30.4	4	4	TP
S104	59.5	46.7	4	3.5	4.1	47.9	30.0	4	4	TP
S005	66.1	151.1	5	4.6	6.0	89.7	32.1	5	4	TP
S050	66.4	160.7	5	4.4	5.9	90.9	32.0	5	4	TP
S083	66.4	9.0	3	4.4	6.9	23.1	23.1	3	3	TN
S021	70.9	15.8	3	4.7	7.6	20.3	20.3	3	3	TN
S106	72.0	12.8	3	5.6	8.5	19.4	19.4	3	3	TN
S080	75.3	25.3	4	6.9	10.8	24.0	24.0	3	3	TN
S007	72.7	13.9	3	7.1	11.1	17.8	17.8	3	3	TN
S089	75.2	9.8	3	7.2	11.5	22.0	17.3	3	3	TN
S081	77.8	15.1	3	8.4	13.9	20.6	20.6	3	3	TN
S101	79.0	12.2	3	4.0	9.1	35.7	30.2	4	4	TP
S098	80.6	11.1	3	6.0	11.2	20.3	19.6	3	3	TN
S084	83.2	18.5	3	8.0	14.1	26.1	26.1	4	4	TP
S079	85.6	12.0	3	8.7	15.0	26.7	26.7	4	4	TP
S087	85.1	6.9	2	5.0	12.3	18.7	18.7	3	3	TN
S015	84.2	8.8	3	11.6	18.0	41.2	19.2	4	3	TP
S086	84.9	10.0	3	8.4	15.6	17.6	17.6	3	3	TN
S073	86.3	16.0	3	9.1	15.6	46.4	20.7	4	3	TP
S10006	88.3	21.2	3	8.4	16.7	28.8	22.6	4	3	TP
S082	88.6	18.5	3	9.5	17.4	22.5	22.5	3	3	TN
S076	89.3	25.8	4	6.9	13.3	35.7	20.4	4	3	TP
S033	90.1	6.1	2	9.4	16.4	30.2	16.6	4	3	FP
S022	88.1	15.1	3	6.0	13.4	67.1	24.2	4	3	TP
S072	90.6	6.1	2	8.7	15.8	34.8	16.5	4	3	FP
S074	90.9	16.4	3	7.7	14.2	63.9	22.3	4	3	TP
S088	94.2	18.8	3	9.7	17.4	65.5	21.8	4	3	TP
S034	97.2	37.7	4	8.5	16.2	40.3	15.8	4	3	TP
S099	97.8	15.8	3	8.7	16.8	73.7	18.6	4	3	TP

FP, false positive; Ir, real intensity scale; Ix, predicted intensity scale; LT, lead time; PGAr, real PGA; PGAx, predicted PGA; *R*, epicenter distance; TN, true negative; TP, true positive.
(Continued next page.)

TABLE 1 (continued)

Performance Summary of the 68 Seismic Stations of the NEEWS during the 2019 Hualien Earthquake

				LT (s)		PGAx (Gal)		Ix		
No.	***R* (km)**	**PGAr (Gal)**	**Ir**	**On-Site**	**Regional**	**On-Site**	**Regional**	**On-Site**	**Regional**	**Classification**
S10005	98.8	11.3	3	10.6	19.1	20.4	13.9	3	3	TN
S096	99.1	25.1	4	9.3	17.6	66.2	28.4	4	4	TP
S114	97.2	12.1	3	7.2	14.5	22.4	22.4	3	3	TN
S018	99.2	11.7	3	10.2	18.5	16.8	16.8	3	3	TN
S107	97.8	20.7	3	8.9	17.2	101.5	18.1	5	3	TP
S115	99.0	9.0	3	6.9	14.5	9.4	8.3	3	3	TN
S085	100.6	10.2	3	10.7	20.5	15.9	15.9	3	3	TN
S078	102.5	11.6	3	9.8	18.7	23.0	15.9	3	3	TN
S071	105.8	11.7	3	9.7	19.7	23.9	18.9	3	3	TN
S070	106.4	14.9	3	11.1	20.6	24.4	22.6	3	3	TN
S102	105.8	6.8	2	9.7	19.6	11.1	11.1	3	3	TN
S024	106.7	52.7	4	8.5	17.4	39.1	18.7	4	3	TP
S077	107.4	33.9	4	10.9	20.2	57.4	20.8	4	3	TP
S111	106.9	21.7	3	7.5	17.1	26.9	14.4	4	3	TP
S095	109.6	27.3	4	11.2	20.9	47.0	13.0	4	3	TP
S100	111.0	38.9	4	11.6	21.5	75.4	13.7	4	3	TP
S108	111.9	55.4	4	10.9	20.9	68.4	23.3	4	3	TP
S027	110.7	6.5	2	11.8	21.4	12.0	12.0	3	3	TN
S075	113.9	13.6	3	11.5	22.0	18.4	18.4	3	3	TN
S10008	115.8	12.2	3	11.9	22.8	41.1	20.6	4	3	TP
S118	114.4	69.1	4	9.3	20.0	40.3	16.8	4	3	TP
S044	116.9	9.1	3	12.2	25.4	15.0	15.0	3	3	TN
S069	119.8	15.6	3	13.2	25.0	27.7	19.5	4	3	TP
S110	120.9	48.1	4	11.6	22.6	33.3	12.9	4	3	TP
S043	121.3	10.6	3	14.1	26.8	16.9	16.9	3	3	TN
S10007	123.5	10.3	3	13.1	25.6	16.9	16.9	3	3	TN
S004	131.9	10.6	3	14.3	28.9	15.9	15.9	3	3	TN
S014	132.9	12.2	3	13.4	27.8	15.7	15.7	3	3	TN
S103	139.6	11.5	3	14.9	29.7	13.8	13.6	3	3	TN
S067	147.6	14.2	3	14.7	31.4	11.5	11.5	3	3	TN
S066	155.5	5.6	2	15.7	34.5	10.5	10.5	3	3	TN
S092	158.4	2.9	2	18.8	40.2	4.8	4.8	2	2	TN
S090	163.8	5.0	2	19.3	41.5	11.0	11.0	3	3	TN

FP, false positive; Ir, real intensity scale; Ix, predicted intensity scale; LT, lead time; PGAr, real PGA; PGAx, predicted PGA; *R*, epicenter distance; TN, true negative; TP, true positive.

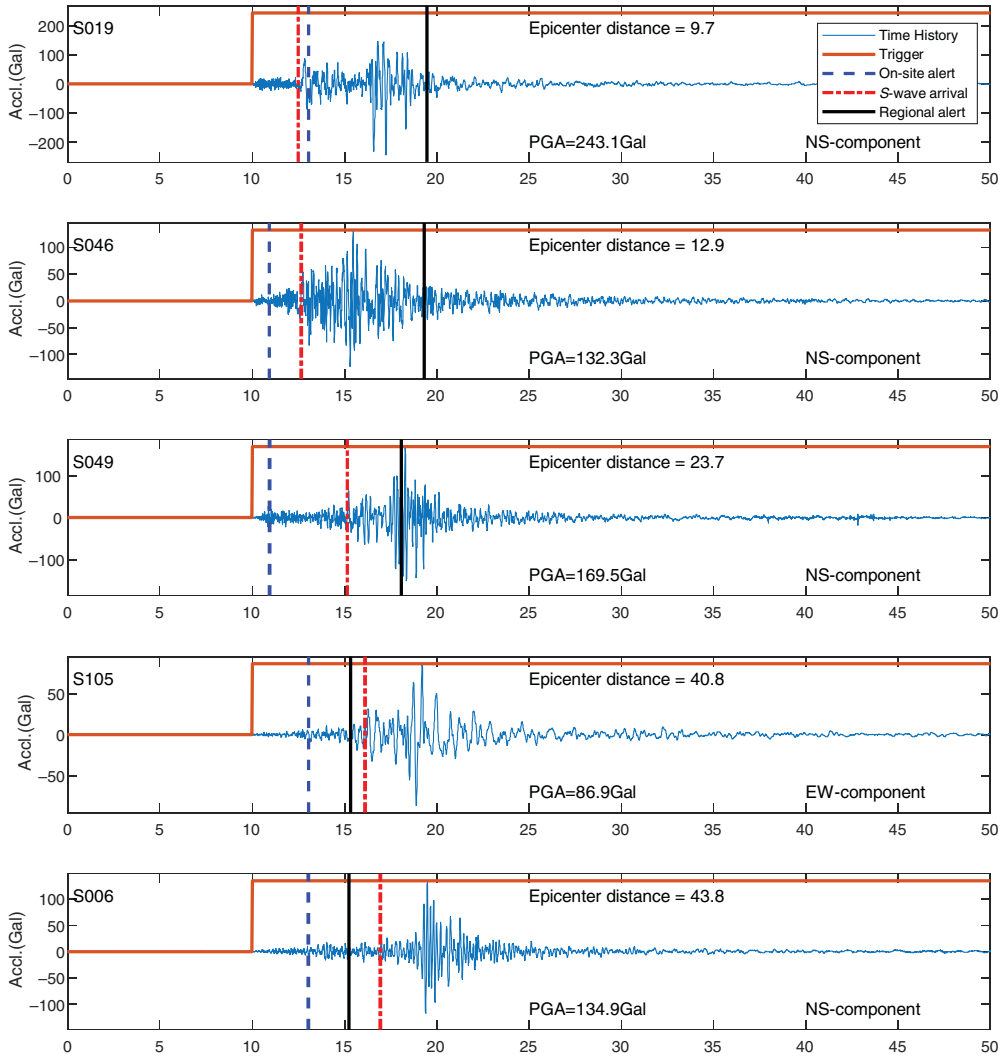

Figure 3. Measured acceleration time history at the 10 stations closest to the epicenter. For conciseness, only the horizontal component with the maximum PGA is plotted in sequence by the epicentral distance. The time when an alert was issued by the on-site approach, time when an alert was issued by the regional approach, and time of arrival of the *S* wave are denoted in dashed blue, solid black, and dash-dotted red lines, respectively. The solid orange envelope represents the phase during which the system was triggered. Part 1: the first 1–5 stations (S019, S046, S049, S105, and S006).

considered it a true positive (TP). Conversely, if an alert was issued but the observed ground motion never reached the threshold, we considered it a false positive (FP). If the final ground motion amplitude reached the threshold but no alerted was issued on time, then we considered it a false negative (FN). If an alert was not issued and the ground motion never reached the threshold, then we considered it a true negative (TN). The confusion matrix of FP, FN, TP, and TN, as shown in Figure 7, is used here to understand the classification performance of the alerts. The alert performance of each station is also summarized in Table 1. Because TN cases were too easily achieved and the number of TN cases was too large (48.5%), in this study, we focused only on the TP, FP, and FN cases.

We calculated two indicators to evaluate the overall performance of the alerts during the 2019 Hualien earthquake: (1) the correct alert rate, CAR = TP/(TP + FP), which is used to answer the question, knowing that an alert has been received, how likely is it that the alert is correct? and (2) the normalized TP rate, TPR = TP/(TP + FN), which is used to answer the question, knowing that an earthquake exceeds the threshold, how likely is it that an alert will be issued? In addition, we also introduced a tolerance range with a scale of ±1 for defining whether a classification was acceptable or not (modified from Meier 2017). As a result, the CAR of the seismic stations was 33/(33+2) = 94.3%, whereas the TPR was 33/(33 +0) = 100%. These results show that the classification performance of the seismic stations of the NEEWS during the 2019 Hualien earthquake was quite promising.

The distribution of the distance between the broadcast stations and the closest seismic stations is illustrated in Figure 8. The average distance is 6.15 km, with a standard deviation of 3.32 km. For most of the broadcast stations in the cities, the distance is only several kilometers. For some of the broadcast stations in the mountain areas, the distance is longer, with the longest distance being 23.5 km. Because there is no literature reporting the performance of EEWSs using satellite approaches, the classification performance of the broadcast stations of the NEEWS for Taiwan is an issue worthy of investigation. However, because the broadcast stations of the NEEWS for Taiwan are not equipped with seismographs, it is difficult to know if the measured seismic intensities actually exceeded the threshold or not, or when the *S* wave arrived at a given station. Therefore, in this study, we simply applied the linear interpolation method to estimate the possible observed PGA values of the broadcast stations from the observed PGA values at all the NEEWS,

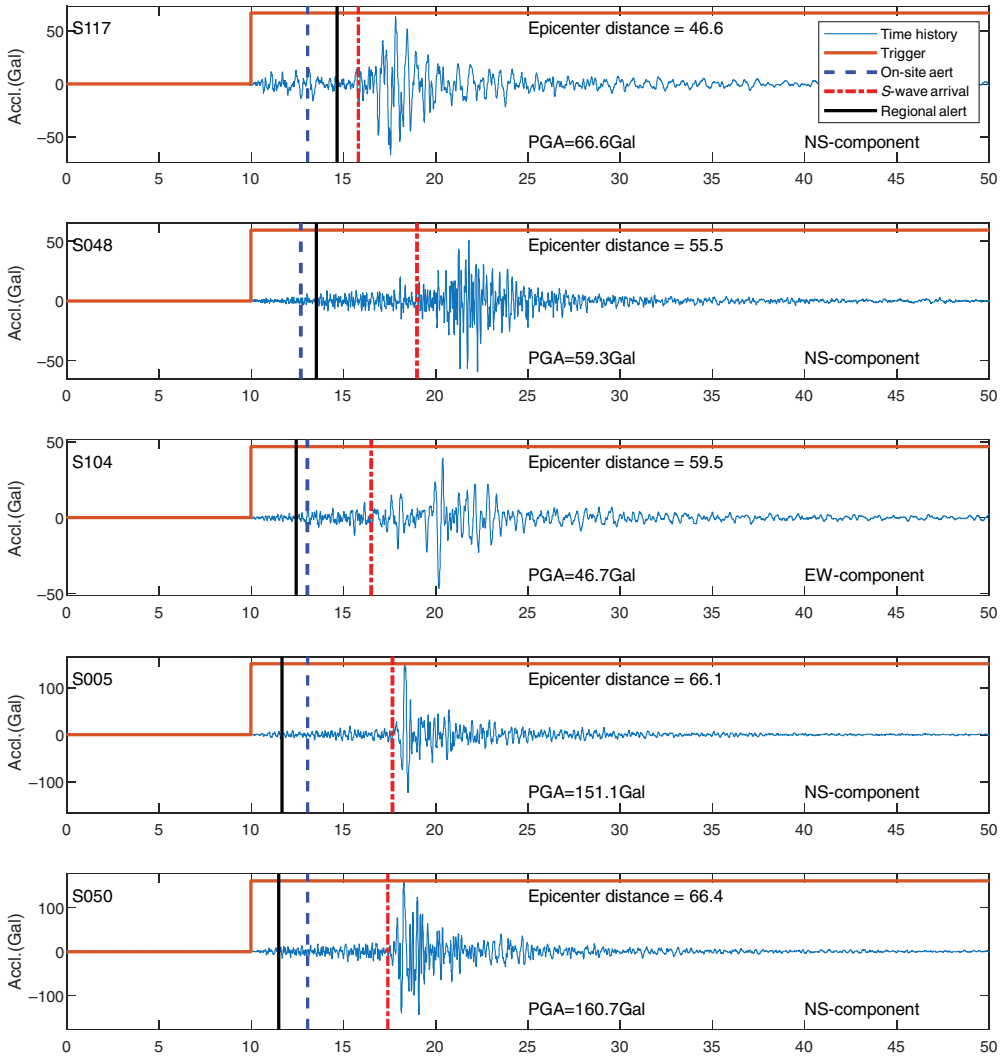

Figure 4. Measured acceleration time history at the 10 stations closest to the epicenter. For conciseness, only the horizontal component with the maximum PGA is plotted in sequence by the epicentral distance. The time when an alert was issued by the on-site approach, time when an alert was issued by the regional approach, and time of arrival of the *S* wave are denoted in dashed blue, solid black, and dash-dotted red lines, respectively. The solid orange envelope represents the phase during which the system was triggered. Part 2: the first 6–10 stations (S117, S048, S104, S005, and S050).

SANTA, P-Alert, and CWB RTD stations (as shown in Fig. 1). The estimated seismic intensity scale values were then calculated using the estimated observed PGA values at the broadcast stations, and then compared with the received predicted intensity scale values of the seismic stations.

As for the LT values of the broadcast stations, we simply used the following equation to estimate the possible LT of each broadcast station LT_S:

$$LT_S = LT_M - (R_M - R_S) \times \kappa, \quad (1)$$

in which LT_M represents the LT of the corresponding seismic station; R_M and R_S represent the epicentral distance of the corresponding seismic station and the broadcast station, respectively; and κ represents the estimated slope of the LT versus epicentral distance in Figure 5. For the broadcast stations with corresponding seismic stations using the on-site approach and the regional approach, κ equals 0.1175 and 0.3058, respectively. The estimated LT values of the broadcast stations are shown in Figure 9. The difference between the estimated LT_S and the real LT values was calculated using $\Delta LT = LT_S - LT_M$, as shown in Figure 10. The average and standard deviation of ΔLT of these broadcast stations were 0.69 s and 2.13 s, respectively, with a maximum and minimum of 9.15 and −7.75 s, respectively. These results indicate that the LT difference of most of the broadcast stations in the cities was only approximately a few seconds, but still that there were some broadcast stations in the mountain areas with larger LT differences. Take the capital city, Taipei, as an example. The average LT of the 509 broadcast stations in Taipei was approximately 17.14 s. The average and standard deviation of ΔLT of these broadcast stations in Taipei were only 0.40 and 1.51 s, respectively.

In addition, note that each broadcast station received a regional alert directly from the CWB, whereas the on-site alert was received from the corresponding seismic stations. Therefore, we were interested in the LT difference of the broadcast stations for the alerts received from the corresponding seismic stations using the on-site approach. The average and standard deviation of ΔLT of the broadcast stations for the received on-site alerts were only 0.11 and 0.68 s, respectively.

Finally, as for the classification performance, the CAR of the broadcast stations was 2124/(2124 + 18) = 99.2%, whereas the TPR of the broadcast stations was 2124/(2124 + 38) = 98.2%. Again, take the capital city, Taipei, as an example. The CAR of the broadcast stations in Taipei was 507/(507 + 2) = 99.6%,

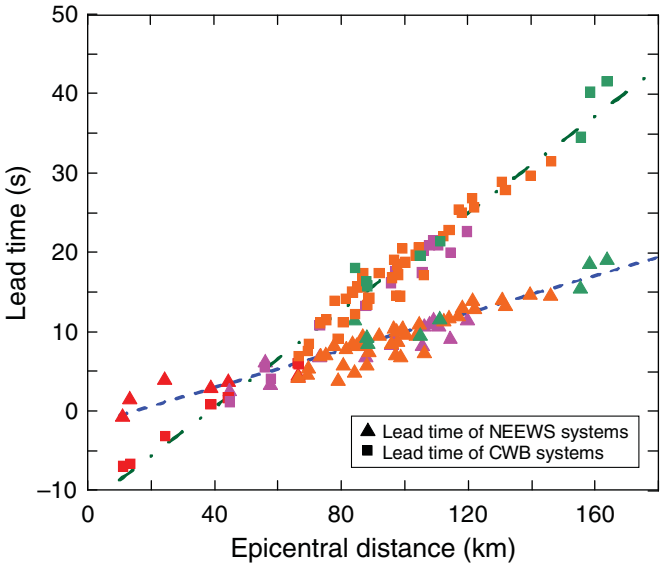

Figure 5. The relationship between lead time (LT) and epicentral distance at the 68 NEEWS seismic stations. Triangles and squares represent the LT values of the on-site and CWB regional approaches, respectively. Blue dashed and green dot-dashed lines indicate the general trend of the on-site approach and CWB regional approach, respectively. Red, pink, orange, and green-colored shapes represent the measured CWB intensities of V, IV, III, and II, respectively.

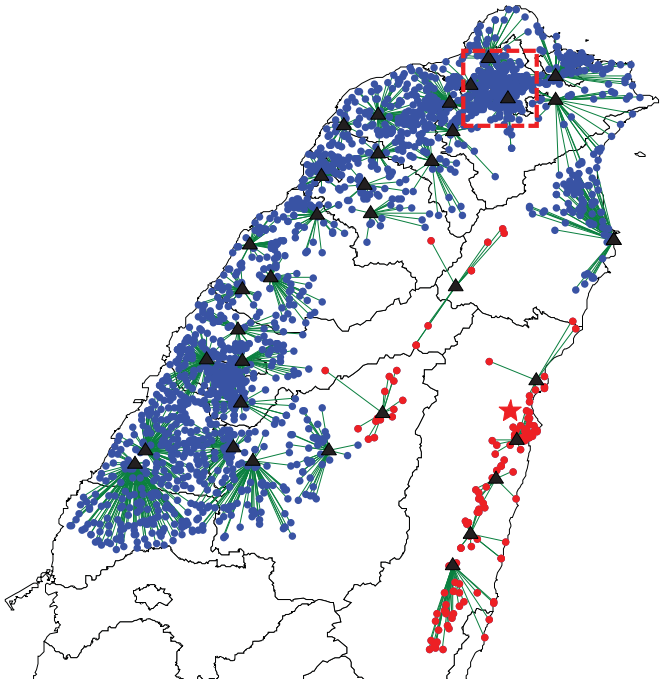

Figure 6. Locations of the 36 NEEWS seismic stations with predicted intensity scale of ≥IV (black triangles) and 2180 corresponding broadcast stations (blue dots). The broadcast stations are connected to the corresponding seismic stations using green lines. The broadcast stations that issued alerts using the on-site approach and regional approach are indicated by red and blue dots, respectively. The location of Taipei is indicated by the red rectangular box.

whereas the TPR of the broadcast stations was 507/(507 + 0) = 100%. These results show that the classification performance of the broadcast stations of the NEEWS during the 2019 Hualien earthquake was also quite promising.

Discussion and Conclusion

In a recent study, Allen and Melgar (2019) summarized the EEWSs that are currently in use around the world. According to their study, there were no EEWSs employing the satellite approach at that time. This article details the NEEWS for schools that was recently established in Taiwan, in addition to providing details regarding the performance of the system during the 2019 M_L 6.3 Hualien earthquake. This moderate earthquake provided an excellent chance to examine the performance of the satellite approach of the NEEWS with respect to an earthquake that resulted in just one fatality and only limited economic loss.

Similar to the original ShakeAlert in the United States (Böse *et al.*, 2011), the broadcast stations of the NEEWS receive alerts from corresponding seismic stations using the on-site approach and from the CWB using the regional approach, and then issue whatever alert is received first. The PGA prediction accuracy for both approaches is quite acceptable, with standard deviation of the logarithm PGA residuals of 0.57 and 0.64 using the on-site approach and the regional approach,

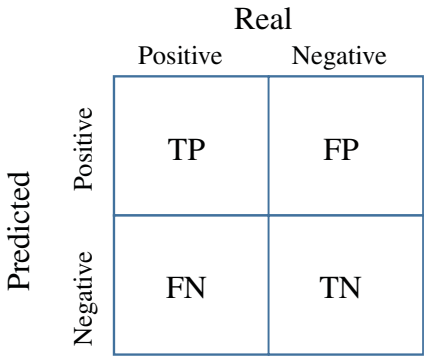

Figure 7. The confusion matrix.

respectively. For the regions with CWB intensity scale of ≥4, the PGA prediction accuracy of the on-site approach is also higher. The hybrid approach and the frame of broadcast stations allow the NEEWS to issue an alert at more than 3500 schools throughout the whole of Taiwan. This cost-effective solution is useful for providing high-density alerts, especially

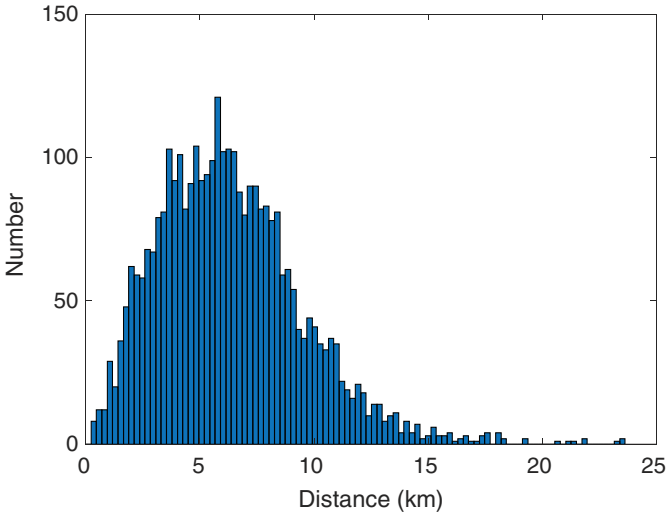

Figure 8. Distribution of the distances between the broadcast stations and the seismic stations. The average distance was 6.15 km, with a standard deviation of 3.32 km.

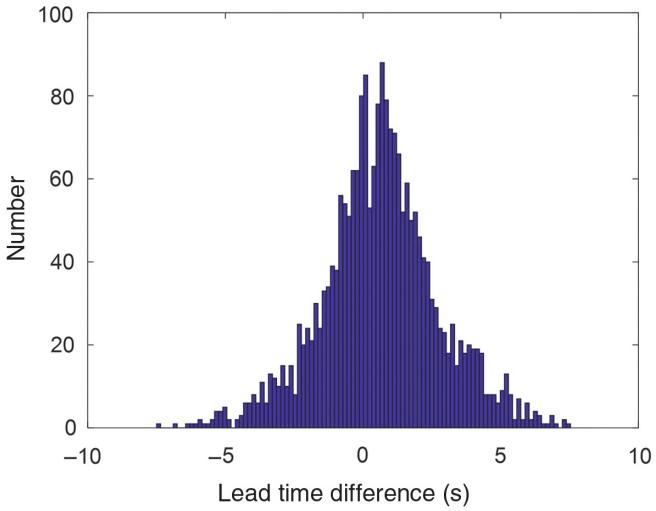

Figure 10. The differences between the estimated LT, LT_S, and the real LT, LT_M, calculated using $\Delta LT = LT_S - LT_M$.

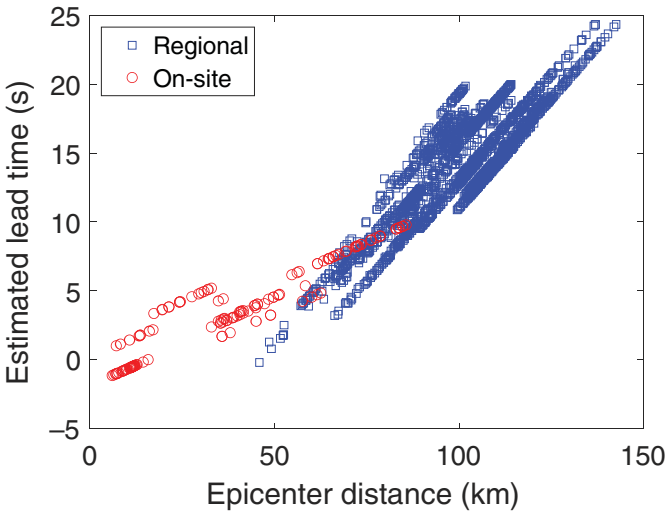

Figure 9. The estimated LT values of the broadcast stations.

for a large region (e.g., California) or country (e.g., India). As for the accuracy of predicted intensity, the performance of the NEEWS during the 2019 Hualien earthquake was quite promising, with IPAR values of 86.1% and 100% for the on-site approach and regional approach, respectively. According to the annual report of the Japan Meteorological Agency (JMA, 2016), the best annual IPAR of the JMA EEWS is 86%. Based on the general trends of the LT values shown in Figure 5, the radii of the blind zone of the on-site approach and the regional approach were approximately 15 and 39 km, respectively. The on-site approach provided faster alerts than the regional approach within a radius of 54 km. In addition, two NEEWS stations that employed a newly updated version of the on-site algorithm demonstrated great potential to increase LT values and narrow the blind zone.

Based on the metrics suggested by Meier (2017), if a reasonable tolerance range was regarded as acceptable, the CAR and TPR of the seismic stations were 94.3% and 100%, respectively. Similarly, based on the estimated PGA and LT values of the broadcast stations, if a reasonable tolerance range was regarded as acceptable, the CAR and TPR of the broadcast stations were 99.2% and 98.2%, respectively. These high values indicate that most of the alerts issued were correct and that most of the stations with intensity scale values larger than the threshold received an alert in time. These results show that, in general, the satellite approach is a promising possible solution for establishing EEWSs for a large number of stations.

In addition, for the capital city, Taipei, which is usually prone to remote large magnitude earthquakes due to its specific basin effect, the average LT was approximately 17.14 s, with the CAR and the TPR of the broadcast stations being 99.6% and 100%, respectively. Evidently, the NEEWS is able to issue correct and fast alerts for the vulnerable capital Taipei in cases of remote earthquakes.

Data and Resources

Data on the acceleration time histories recorded by the Central Weather Bureau real-time data stream (CWB RTD) stations and the National Center for Research on Earthquake Engineering (NCREE) earthquake early warning system (NEEWS) stations can be obtained from the Civil IoT Taiwan Data Service Platform at ci.taiwan.gov.tw (last accessed October 2019). Data on the acceleration

time histories recorded by the SANTA stations can be obtained from the Seismic Array of NCREE in Taiwan at santa.ncree.org (last accessed October 2019). Data on the acceleration time histories recorded by the *P*-Alert Strong Motion Network can be obtained at palert.earth.sinica.edu.tw (last accessed October 2019).

References

Allen, R. M., and D. Melgar (2019). Earthquake early warning: Advances, scientific challenges, and societal needs, *Annu. Rev. Earth Planet. Sci.* **47**, 361–388.

Allen, R. M., P. Gasparini, O. Kamigaichi, and M. Böse (2009). The status of earthquake early warning around the world: An introductory overview, *Seismol. Res. Lett.* **80**, 682–693.

Böse, M., E. Hauksson, M. Hellweg, G. Cua, and CISN EEW Group (2011). CISN ShakeAlert: UserDisplay – Operations Guide V3, SeismoLab, California Institute of Technology, Pasadena, California.

Böse, M., T. Heaton, and E. Hauksson (2012). Rapid estimation of earthquake source and ground-motion parameters for earthquake early warning using data from a single three-component broadband or strong-motion sensor, *Bull. Seismol. Soc. Am.* **102,** no. 2, 738–750.

Carranza, M., E. Buforn, S. Colombelli, and A. Zollo (2013). Earthquake early warning for southern Iberia: A P wave threshold-based approach, *Geophys. Res. Lett.* **40,** no. 17.

Caruso, A., S. Colombelli, L. Elia, M. Picozzi, and A. Zollo (2017). An on-site alert level early warning system for Italy, *J. Geophys. Res.* **122,** no. 3, 2106–2118.

Chen, D. Y., N. C. Hsiao, and Y. M. Wu (2015). The Earthworm based earthquake alarm reporting system in Tai7wan, *Bull. Seismol. Soc. Am.* **105**, 568–579.

Chen, D. Y., Y. M. Wu, and T. L. Chin (2015). Incorporating low-cost seismometers into the Central Weather Bureau seismic network for earthquake early warning in Taiwan, *Terr. Atmos. Ocean. Sci.* **26**, 503–513.

Emolo, A., M. Picozzi, G. Festa, C. Martino, S. Colombelli, A. Caruso, L. Elia, A. Zollo, P. Brondi, and N. Miranda (2016). Earthquake early warning feasibility in the Campania region (southern Italy) and demonstration system for public school buildings, *Bull. Earthq. Eng.* **14,** no. 9.

Hsu, T. Y., S. K. Huang, Y. W. Chang, C. H. Kuo, C. M. Lin, T. M. Chang, K. L. Wen, and C. H. Loh (2013). Rapid on-site peak ground acceleration estimation based on support vector regression and P-wave features in Taiwan, *Soil Dynam. Earthq. Eng.* **49**, 210–217.

Hsu, T. Y., P. Y. Lin, H. H. Wang, H. W. Chiang, Y. W. Chang, and C. H. Kuo (2018). Comparing the performance of the NEEWS earthquake early warning system against the CWB system during the 6 February 2018 M_w 6.2 Hualien earthquake, *Geophys. Res. Lett.* **45**, 6001–6007.

Hsu, T. Y., H. H. Wang, P. Y. Lin, C. M. Lin, C. H. Kuo, and K. L. Wen (2016). Performance of the NCREE's on-site warning system during the 5 February 2016 M_w 6.53 Meinong earthquake, *Geophys. Res. Lett.* **43**, 8954–8959.

Japan Meteorological Agency (JMA) (2016). JMA operational evaluation report, JMA (in Japanese).

Jean, W. Y., Y. W. Chang, K. L. Wen, and C. H. Loh (2006). Early estimation of seismic hazard for strong earthquakes in Taiwan, *Nat. Hazards* **37**, 39–53.

Kanamori, H. (2005). Real-time seismology and earthquake damage mitigation, *Annu. Rev. Earth Planet. Sci.* **33**, 195–214.

Kuo, C. H., J. Y. Huang, C. M. Lin, T. Y. Hsu, S. H. Chao, and K. L. Wen (2019). Strong ground motion and pulse-like velocity observations in the near-fault region of the 2018 M_w 6.4 Hualien, Taiwan earthquake, *Seismol. Res. Lett.* **90,** no. 1, 40–50.

Meier, M. A. (2017). How "good" are real-time ground motion predictions from Earthquake Early Warning systems? *J. Geophys. Res.* **122,** no. 7, 5561–5577.

Nakamura, Y. (1998). A new concept for the earthquake vulnerability estimation and its application to the early warning system, *Proc. Early Warning Conf.*, Potsdam, Germany, 693–699).

Odaka, T., K. Ashiya, S. Tsukada, S. Sato, K. Ohtake, and D. Nozaka (2003). A new method of quickly estimating epicentral distance and magnitude from a single seismic record, *Bull. Seismol. Soc. Am.* **93,** no. 1, 526–532.

Peng, C., J. Yang, Y. Chen, X. Zhu, Z. Xu, Y. Zheng, and X. Jiang (2015). Application of a threshold-based earthquake early warning method to the M_w, 6.6 Lushan Earthquake, Sichuan, China, *Seismol. Res. Lett.* **86,** no. 3, 841–847.

Wu, Y. M., D. Y. Chen, T. L. Lin, C. Y. Hsieh, T. L. Chin, W. Y. Chang, and S. H. Ker (2013). A high-density seismic network for earthquake early warning in Taiwan based on low cost sensors, *Seismol. Res. Lett.* **84,** no. 6, 1048–1054.

Wu, Y. M., W. H. K. Lee, C. C. Chen, T. C. Shin, T. L. Teng, and Y. B. Tsai (2000). Performance of the Taiwan Rapid Earthquake Information Release System (RTD) during the 1999 Chi-Chi (Taiwan) earthquake, *Seismol. Res. Lett.* **71**, 338–343.

Wu, Y. M., T. L. Teng, T. C. Shin, and N. C. Hsiao (2003). Relationship between peak ground acceleration, peak ground velocity, and intensity in Taiwan, *Bull. Seismol. Soc. Am.* **91,** no. 5, 1218–1228.

Zollo, A., O. Amoroso, M. Lancieri, Y. M. Wu, and H. Kanamori (2010). A threshold-based earthquake early warning using dense accelerometer networks, *Geophys. J. Int.* **183**, 963–974.

Manuscript received 28 October 2019
Published online 4 November 2020